JGR Biogeosciences

METHOD
10.1029/2025JG009197

Characterization of the Nature of Organic Matter in Carbonate Rocks: Implications for Geological and Environmental Studies

Alicia Moya[1,2], Rajkumar Chowdhury[2,3,4], Yves Perrette[5], Fabienne Giraud[2], Laurent Charlet[2], Christophe Sandt[6], Hugo Chauvet[7], Frederic Jamme[7], Alexander Van Driessche[2,8], and Alejandro Fernandez-Martinez[2]

[1]Applied Physical Chemistry Department, Universidad Autónoma de Madrid, Madrid, Spain, [2]University Grenoble Alpes, University Savoie Mont Blanc, CNRS, IRD, IFSTTAR, ISTerre, Grenoble, France, [3]LGL-TPE - UCB, Lyon1 - UJF - UMR CNRS 5276 - ENS de Lyon - 46, Lyon Cedex 07, France, [4]Pôle d'Etudes et de Recherche de Lacq, TotalEnergies, Lacq, France, [5]University Savoie Mont Blanc, CNRS, EDYTEM, Le Bourget du Lac, France, [6]Synchrotron SOLEIL, SMIS beamline, L'Orme des Merisiers, Gif-sur-Yvette, France, [7]Synchrotron SOLEIL, DISCO beamline, L'Orme des Merisiers, Gif-sur-Yvette, France, [8]Instituto Andaluz de Ciencias de la Tierra (IACT), CSIC – University of Granada, Granada, Spain

Key Points:

- Heterogeneous organic matter distribution in carbonate rocks is influenced by depositional environments and diagenetic processes
- Specific bioclast types can be identified by the fluorescence signatures of their organic content
- Fluorescence of small biomolecules correlates with nanoscale wettability, underscoring the role of biomolecules in governing fluid behavior in carbonates

Supporting Information:

Supporting Information may be found in the online version of this article.

Correspondence to:

A. Moya,
alicia.moya@uam.es

Citation:

Moya, A., Chowdhury, R., Perrette, Y., Giraud, F., Charlet, L., Sandt, C., et al. (2026). Characterization of the nature of Organic matter in carbonate rocks: Implications for geological and environmental studies. *Journal of Geophysical Research: Biogeosciences*, *131*, e2025JG009197. https://doi.org/10.1029/2025JG009197

Received 17 JUN 2025
Accepted 14 FEB 2026

Author Contributions:

Conceptualization: Alicia Moya, Frederic Jamme, Alexander Van Driessche, Alejandro Fernandez-Martinez
Data curation: Alicia Moya
Formal analysis: Alicia Moya
Funding acquisition: Alicia Moya
Investigation: Alicia Moya, Rajkumar Chowdhury, Yves Perrette, Fabienne Giraud, Christophe Sandt, Hugo Chauvet, Frederic Jamme, Alexander Van Driessche, Alejandro Fernandez-Martinez
Methodology: Alicia Moya, Christophe Sandt, Hugo Chauvet

Abstract Organic matter in carbonate rocks plays a crucial role in processes such as fluid flow regulation, carbon sequestration, contaminant transport, and hydrocarbon recovery. This study employed multimodal spectroscopic techniques, including fluorescence imaging and Fourier transform infrared (FTIR) spectroscopy, to characterize the spatial distribution and spectral characteristics of organic matter in carbonate rocks by comparing bioclastic and non-bioclastic components. Fluorescence hyperspectral analysis revealed heterogeneous distribution within the carbonate framework. UV fluorescence appears preferentially associated with bioclastic grains, whereas visible fluorescence is more broadly distributed and more pronounced in reservoir samples. Variations in spectral features, including differences in the relative contributions of tyrosine- and tryptophan-like emission, highlight contrasts among bioclastic components such as red algae and mollusks and reveal the critical role of biominerals in tunning surface chemistry and wettability. These findings highlight the heterogeneity and complexity of organic matter in carbonate rocks, offering insights into diagenesis, organic matter preservation, and paleoenvironmental reconstructions with implications for rock characterization and resource management. FTIR microspectroscopy provides complementary information on organic functional groups and supports the heterogeneous distribution of organic matter inferred from fluorescence mapping. While these spectroscopic signatures do not provide direct molecular identification, the combined spatial and spectral observations suggest that preserved or altered organic matter contributes to variations in surface chemistry and wettability in carbonate rocks. These results underscore the complexity of organic matter preservation in carbonates and demonstrate the potential of fluorescence hyperspectral imaging as a framework for future method validation studies addressing carbonate diagenesis, paleoenvironmental reconstruction, and reservoir characterization.

Plain Language Summary Carbonate rocks, which make up a significant part of Earth's crust, contain organic matter that influences important processes such as carbon storage, fluid movement, and resource management. This study used advanced imaging and synchrotron-based spectroscopy techniques to analyze how organic matter is distributed within these rocks and how biological materials contribute to their chemistry. Outcomes of this research reveal that tyrosine and tryptophan amino acids serve as markers of biological origin, helping to distinguish fossilized materials. Differences in these organic components impact the surface properties of the rocks, affecting how they interact with fluids and other substances. These insights improve our understanding of how rocks evolve over time, preserve organic materials, and provide crucial data for environmental studies, fossil research, and industries that rely on rock characterization.

1. Introduction

Carbonate rocks are a key component of sedimentary systems, preserving fossils of a rich variety of marine and terrestrial life forms, which serve as invaluable repositories of Earth's geological history (Boggs, 2006). Indeed, the distribution, composition, and relative abundance of bioclastic (skeletal fossil fragments) and non-bioclastic (abiotic mineral constituents) grains, and the diagenetic alteration of organic matter, all significantly influence the

Project administration: Alicia Moya
Resources: Alexander Van Driessche, Alejandro Fernandez-Martinez
Supervision: Alicia Moya
Writing – original draft: Alicia Moya
Writing – review & editing: Alicia Moya, Yves Perrette, Christophe Sandt, Hugo Chauvet, Frederic Jamme, Alexander Van Driessche, Alejandro Fernandez-Martinez

physicochemical properties of carbonate rocks, thereby impacting their behavior in geological processes. Beyond their geological significance, carbonate rocks play a crucial role in the global carbon cycle, acting as both atmospheric carbon dioxide (CO_2) sinks and mediators of organic matter stabilization (Martin, 2017; Xu & Tsang, 2024). These organic compounds originate from both biotic and abiotic sources, including degradation products of microbial communities, plants, and animals, as well as insoluble organic matter (Bisse et al., 2022; Jin & Zimmerman, 2010; Meyers, 1997). Organic compounds can also be found in carbonate rocks as remains of original organisms preserved through fossilization. The complexity and heterogeneity of organic components within carbonate rocks are influenced by biological, physicochemical, burial, and depositional factors (Bjørlykke, 2014; Konhauser, 2009).

Unraveling the intricate interfacial properties of carbonate rocks requires identifying and characterizing the biogenic remains preserved within them, as these are inherently linked to the type and quantity of organic matter embedded in the mineral matrices. The interactions between carbonate minerals, particularly Ca^{2+} ions, and organic matter play a key role in fluid transport, facilitating the entrapment and long-term stabilization of organic compounds (Ma et al., 2024; Tong et al., 2024). This process is essential for the long-term carbon sequestration, as it governs organic matter retention, transport and recalcitrance (resistance to degradation) (Harms et al., 2021; Pessarrodona et al., 2023). These organic components modify the interfacial properties of carbonate rocks, affecting how fluids interact with the rock surface and influencing processes such as rock alteration, carbon storage, and environmental dynamics. In a previous study, we investigated the wettability properties of carbonate rocks from the micro-to nano-scale, revealing preferentially hydrophobic areas within the bioclastic components (Moya et al., 2023). These findings highlight how organic matter influences surface energy and fluid adhesion, with broader implications for carbon sequestration, rock weathering, and subsurface fluid dynamics. Therefore, a deeper understanding of the complex physicochemical properties of the carbonate rocks and their interactions is paramount for predicting rock behavior in geological systems, environmental remediation, and groundwater management (Lim et al., 2010; Ridgwell & Zeebe, 2005).

In this context, synchrotron radiation spectroscopic techniques, such as Deep-Ultraviolet (SR-DUV) fluorescence and Fourier transform infrared (SR-FTIR) spectroscopy, offer powerful tools for identifying the type, composition, and spatial distribution of organic matter within carbonate rocks (Bunkin et al., 2023; Ménez et al., 2018). In particular, SR-DUV fluorescence spectroscopy enables the selective excitation of specific fluorescent organic compounds, revealing two distinct fluorescence signals: (a) a protein-like fluorescence with emission in the 300–350 nm range, which is commonly associated with aromatic amino acids (phenylalanine, tyrosine, and tryptophan) present as protein constituents, free molecules, or degradation residues; and (b) an aliphatic-like fluorescence, emitting in the visible range (420–450 nm) and associated with molecules of low-to-high molecular weight (Coble, 1996). Among amino acids, phenylalanine (with a phenyl group and emission maximum of 282 nm), tyrosine (with a phenol group and emission center at 303 nm), and tryptophan (with an indole group and emission center at 350 nm) are the primary contributors to UV fluorescence (Lakowicz, 2006). These amino acids are inherently hydrophobic, and given our previous findings of preferential fluorescence and hydrophobicity in bioclastic grains, their presence and spatial distribution provide crucial insights into wetting heterogeneities in carbonates and on the stabilization of organic matter in carbonate rocks.

Complementary to UV spectroscopy, FTIR spectroscopy enables the determination of organic functional groups, providing valuable insights into organic matter degradation and maturation (Loron et al., 2022). For instance, the identification of amide bonds in FTIR spectra indicates protein preservation while their absence the degradation into amino acids (Chiriboga et al., 1998), possibly due to diagenetic processes. However, carbonates also present IR vibrations in the 1,500–1,400 cm^{-1} region (Rodriguez-Blanco et al., 2011), which overlaps with the signals from common organic functional groups (Khan et al., 2018). In this sense, the development of spectral deconvolution and fitting techniques, or analysis such as Principal Component Analysis (PCA) of the spectral data, can help in the identification of specific functional groups (Pâris et al., 2011; Pisapia et al., 2018). In summary, high-resolution measurements in synchrotron facilities enable spectral mapping at micrometric scales, providing quantitative information about the distribution and abundance of organic matter within carbonate constituents.

This study employs synchrotron-based fluorescence and infrared spectroscopy to map the distribution of organic matter within carbonate rocks thin section, focusing specifically on limestones rich in bioclastic grains. The carbonate rock samples investigated in this study, including non-reservoir and reservoir-depleted rocks, were selected based on their abundancy of bioclastic grains and different hydrocarbon content (see Supplementary

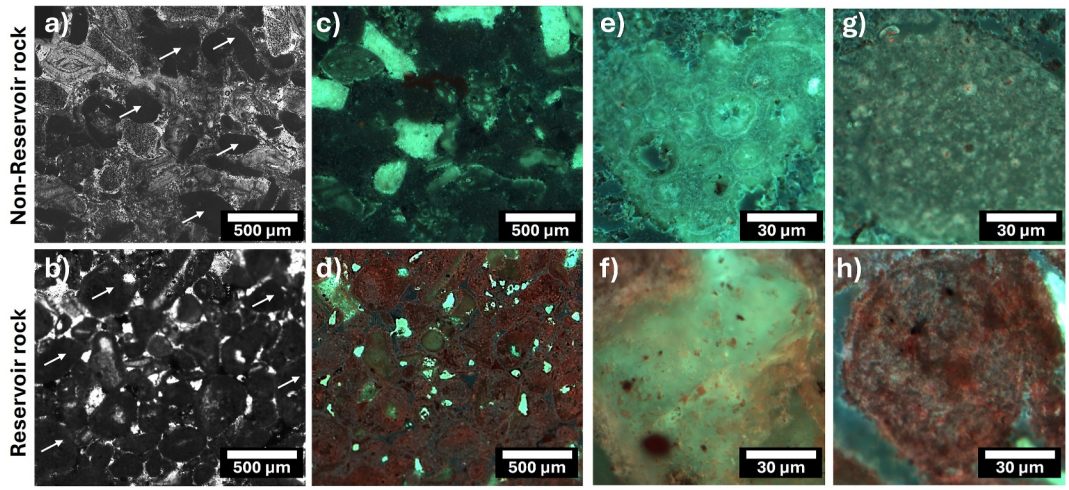

Figure 1. Low magnification filtered-emission fluorescence images. (a)–(b) Optical microscope images at low magnification (10X) with white arrows indicating the non-bioclastic grains in (a) Non-reservoir and (b) Reservoir carbonate rock. (c)–(d) Corresponding full-field filtered-fluorescence RGB composite images (R = 420–480 nm, G = 352–388 nm, and B = 329–351 nm) in (c) Non-reservoir and (d) Reservoir carbonate rock. (e)–(h) Higher magnification (40X) RGB fluorescence images of (e) Bioclastic grains in Non-reservoir rock, (f) Bioclastic grains in Reservoir rock, (g) Non-bioclastic grains in Non-reservoir rock and (h) Non-bioclastic grains in Reservoir rock.

Information S1 for more details). Furthermore, in a prior investigation, we elucidated the role of the biogenic origin of minerals in the wettability properties of different carbonate rocks at the nanoscale (Moya et al., 2023). Building upon these findings, we hypothesized that the content and type of bioclastic and non-bioclastic grains could regulate the wettability properties of carbonate-water interfaces. To test this hypothesis, our analyses focused on evaluating the differences in organic matter composition of these rocks. The micrometer to nanometer scale data provide new insights into the relationship between organic compound distribution and rock wettability. These results will enhance our ability to predict fluid-rock behavior in geological processes, with implications for both fundamental geological research on diagenesis and fluid transport, as well as applied CO_2 cycling rates or reservoir management.

2. Results

2.1. Multidimensional Spectroscopic Analysis of Non-Reservoir and Reservoir Carbonate Rocks

The spatial distribution of fluorescent species within preselected rock samples (see Mat & Met) was mapped using DUV fluorescence, with monochromatized synchrotron light at an excitation wavelength of 275 nm, and employed five emission filters, covering a broad spectrum of the UV-visible emission spectra (329–607 nm). Figure 1 illustrates the analysis of thin sections of the Non-reservoir (top) and Reservoir (bottom) carbonate rocks at low magnification (10X), containing a multitude of bioclastic and non-bioclastic grains. These components were previously identified and characterized by cross-polarized optical microscopy, before performing the spectroscopy measurements. The optical images (Figures 1a and 1b) are presented in greyscale, whereas the fluorescence images (Figures 1c and 1d) are presented in RGB scale. The intensity of each RGB channel was equally fixed for the three channels to min/max values of 0/2,500 and 0/8,000 for images acquired at 10X and 40X, respectively. Given the intensity of fluorescence below 500 nm, the RGB images are formed by the combination of three fluorescence-filtered images: red corresponds to the fluorescence bandpass filter in the range of 420–480 nm, green of 352–388 nm, and blue of 329–351 nm.

A comparison of the fluorescence images of the Non-reservoir and Reservoir rocks reveals differences in the fluorescence signals between both rock types. Notably, the Reservoir rock exhibits higher fluorescence intensity and fluorescence signal of a different chemical nature compared to the Non-reservoir rock, as indicated by a predominantly red coloration in the RGB image. In the Non-reservoir rock, the green coloration of the RGB image represents a UV fluorescence emission in the range of 352–388 nm and is primarily observed in bioclastic grains. The non-bioclastic grains (highlighted with white arrows) appear dark due to a weak or absent fluorescence

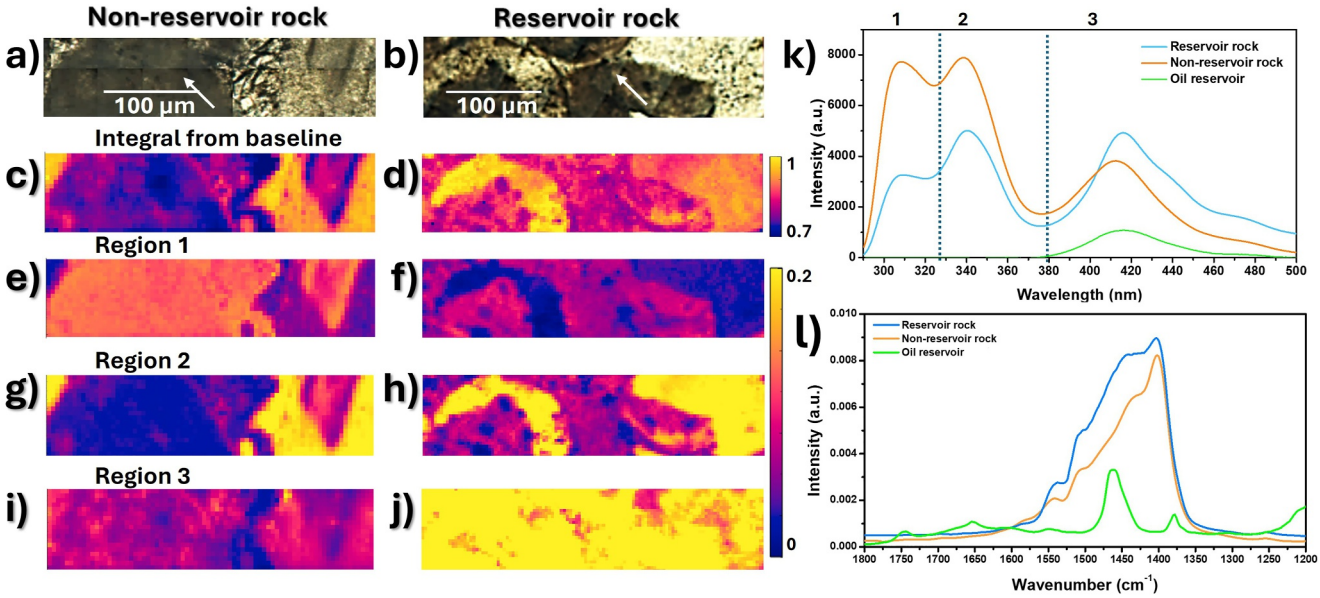

Figure 2. Fluorescence spectral mapping of Non-reservoir and Reservoir rocks. (a–b) Optical images of the Non-reservoir (left) and Reservoir (right) rock, with white arrows on dark grains corresponding non-bioclastic grains (c–d) Corresponding fluorescence intensity maps from the spectra integration from the baseline with a resolution of 5 µm. (e–j) Fluorescence intensity maps obtained from the integration of Regions 1–3, highlighted in (k) representative fluorescence spectra of carbonate rocks together with the spectrum of the oil reservoir.

signal. In contrast, fluorescence signals in the Reservoir rock are detected across all grains, with emission centers shifted to higher wavelengths in the visible range. While well-preserved bioclastic grains exhibit similar fluorescence signals to those in the Non-reservoir rock (green coloration), the non-bioclastic grains present fluorescence at higher wavelengths, specifically in the region 420–480 nm (red coloration). This suggests the presence of different types of organic molecules in the non-bioclastic than in the bioclastic grains of the reservoir rock. Importantly, both samples demonstrate significant heterogeneity in the fluorescence signal intensity, with areas of higher fluorescence intensity corresponding to fragments from identified biomineral remains (bioclastic grains).

Higher-magnification images (40X) provided detailed insights into the fluorescence characteristics of bioclastic (Figures 1e and 1f) and non-bioclastic grains (Figures 1g and 1h) of both rock types. In the Non-reservoir rock, the fluorescence signal within bioclastic grains presents a uniform green coloration, indicating that the bioclastic grains present mostly fluorescence at lower wavelengths, specifically, in the UV range. However, in the Reservoir rock, the outer part of the bioclastic grain in Figure 1f exhibits fluorescence at higher wavelengths, in the visible range, manifesting as a pale red coloration in the RGB fluorescence image. Notably, in non-bioclastic grains of the Reservoir rock, this red fluorescence (wavelength range between 420 and 480 nm) predominates, and interestingly, it also appears in the peloids (non-bioclastic grains) of the Non-reservoir, particularly within the pore spaces (see corresponding visible images in Figure S1 in Supplementary Information S1).

After analyzing the fluorescence signal of Non-reservoir and Reservoir rock samples at various spatial scales, we employed a fluorescence hyperspectral (point-scanning) microscope to obtain higher spectral information, with high spatial resolution, from the most relevant regions of each rock. Figure 2 shows optical images of the Non-reservoir (Figure 2a and Figure S2a in Supplementary Information S1) and Reservoir rocks (Figure 2b and Figure S2b in Supplementary Information S1). Using an excitation wavelength of 275 nm, fluorescence mapping spectra were acquired, revealing non-homogeneous UV fluorescence emission spectra on the surfaces of the carbonate rocks, especially in the Non-reservoir rock. Integrating the fluorescence intensity from the baseline (Figures 2c and 2d), the spectral maps obtained for each carbonate rock exhibit a higher intensity signal in the bioclastic grains compared to the non-bioclastic grains. However, among the non-bioclastic grains highlighted with white arrows, much higher fluorescence intensity was observed for those of the Reservoir rock, while those in the Non-reservoir rock showed very low fluorescence intensity (cf. Figure 2). Since the thin section samples were identically

prepared keeping the same thickness, the fluorescence results suggest a correlation between the fluorescence intensity and the intrinsic properties of each grain.

The average fluorescence spectra of each rock sample (5,202 spectra for Non-Reservoir rock and 14,800 spectra for Reservoir rock) are presented in Figure 2k and Figure S3 in Supplementary Information S1, delineated into three distinct emission regions labeled 1–3. Region 1 and 2 correspond to fluorescence in the UV range, specifically within the wavelength ranges of 290–325 and 325–375 nm, respectively. This UV fluorescence appears heterogeneously distributed in both rocks. Although the signals from Region 1 and 2 require further analysis (see below) the fluorescence signal of Region 3 (375–500 nm range) can be potentially attributed to aliphatic-rich compounds including crude oil (see its emission spectra centered at 415 nm in Figure 2k). (Liu et al., 2020) It is noteworthy that other bands can also contribute to the fluorescence intensity signal in the visible range such as the intrinsic calcite emission or that originated by the presence of metal impurities, which typically occurs in the range of 400–700 nm (Toffolo et al., 2019). However, both rocks have very similar compositions in terms of mineralogy and chemistry (see Table S1 and S2 in Supplementary Information S1), being Sr and Mn the main inorganic impurities. These impurities can generate lattice defects by substituting Ca atoms in calcite, leading to fluorescence above 500 nm (not observed in our measurements). These results suggest that the main difference between both rocks is due to the amount and diversity of preserved organic matter.

To discern the spatial distribution of the main fluorescence contribution of the rock components, Figures 2e–2j illustrates area maps for regions 1–3. Regions 1, below 320 nm (Figures 2e and 2f), characteristic of the non-bioclastic grains, are more prominent in the Non-reservoir rock. Fluorescence emission around 340 nm (Region 2) is predominantly observed in the bioclastic grains of both Non-reservoir and Reservoir rocks (Figures 2g and 2h). This UV fluorescence may correspond to small aromatic molecules, potentially of biological origin. Finally, the spatial maps for Region 3 (Figures 2i and 2j) confirm that visible fluorescence is more characteristic of the Reservoir rock, both in bioclastic and non-bioclastic grains. This aliphatic-like fluorescence signal is distributed along the carbonate rock and is likely to be responsible for crude oil adsorption. This finding aligns with the higher intensity observed in this region for the Reservoir rock, further corroborating the results obtained from previous fluorescence images (Figure 1).

Based on the fluorescence results, the same limestone thin sections were further analyzed using IR spectroscopy to obtain complementary information about the organic matter present in the carbonate rocks. In the range of 1,600–1,350 cm^{-1} (Figure 2l), the signals of calcite particles (Table S1 in Supplementary Information S1) for both carbonate rocks overlap with the vibrations of the organic functional groups (Matei et al., 2020). Thus, a fitting analysis of these carbonate IR spectra was conducted using 7 components with centers around 1,396, 1,412, 1,436, 1,465, 1,510, 1,545, and 1,585 cm^{-1} (see Figure S4 in Supplementary Information S1 and corresponding assignment in Table S3 in Supplementary Information S1). The carbonate stretching vibrations in calcite, appearing at 1,500–1,400 cm^{-1} (Rodriguez-Blanco et al., 2011; Wada et al., 2018), constitute the primary contribution to the IR spectra of both rocks. Minor contributions in the range of 1,600–1,500 cm^{-1} can be attributed to aromatic C=C and C=N signals, chemical features characteristic of aromatic organic matter (Coates, 2006). Furthermore, the absence of IR absorption in the range 1,800 and 1,600 cm^{-1} indicates that amide and carbonyl bonds are not the main organic matter in the carbonate rocks. Instead, small molecules such as amino acids or their derivatives could be preserved. Finally, the higher IR intensity of the Reservoir rock compared to the Non-reservoir rock can be attributed to the contribution of the oil remains in the Reservoir rock, which presents the most intense signal at 1,465 cm^{-1} (Figure 2l).

2.2. Elucidating the Nature of Biotic Organic Matter in Non-Reservoir and Reservoir Rocks

The fluorescence spectra collected between 290 and 500 nm after excitation at 275 nm were analyzed to elucidate the different compositions of the organic matter. The average spectra resulting from bioclastic ($N = 1,742$ spectra for Non-reservoir and $N = 6,442$ spectra for Reservoir rock) and non-bioclastic grains ($N = 3,423$ spectra for Non-reservoir and $N = 8,358$ spectra for Reservoir rock) exhibit again clear differences between both rocks. As shown in Figure 3a, the fluorescence intensity in the visible range (around 415 nm) is more significant for the Reservoir rock, with a broader emission toward higher wavelengths, compared to the Non-reservoir rock. Notably, this signal is independent of the carbonate grain type and can be attributed to the adsorption of crude oil. Figure 3a also reveals differences in the UV fluorescence intensity depending on the rock composition, distinguishing between non-bioclastic and bioclastic grains. Non-bioclastic grains exhibit contributions centered at 310 and 340 nm with

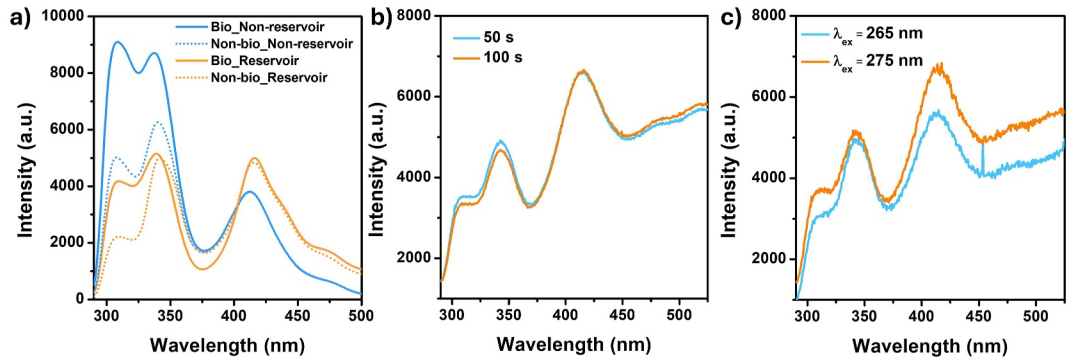

Figure 3. Fluorescence spectra of Non-reservoir and reservoir rocks under different conditions. (a) Representative fluorescence spectra of bioclastic (blue) and non-bioclastic grains (orange) in Non-reservoir (solid lines) and Reservoir (dotted lines) carbonate rocks. (b) Fluorescence spectra of Non-reservoir rock at different time exposition to UV light excited at 275 nm. (c) Fluorescence spectra of Non-reservoir rock at 5 s of acquisition time of UV light exposition of 265 and 275 nm.

lower UV fluorescence intensity than bioclastic grains. Interestingly, the emission at 340 nm of the bioclastic grains is shifted to lower wavelengths in comparison with that of the non-bioclastic grains.

Fluorescence spectroscopy is sensitive to small aromatic compounds, which in geological samples, such as carbonate rocks, are often derived from the degradation of primary organic material such as proteins. In this context, the fluorescent aromatic amino acids (phenylalanine, tyrosine, and tryptophan) play a key role, as they degrade into smaller aromatic compounds that also contribute to the observed fluorescence. In our experiments with an excitation wavelength of 275 nm, mainly tyrosine and tryptophane molecules can be excited (see Figure S5 in Supplementary Information S1). To better understand the sources and nature of these signals, we conducted experiments aimed at identifying and characterizing these molecular components under UV excitation. Tyrosine and tryptophan amino acids can undergo further UV induced degradation into phenol, *p*-cresol, and indole derivatives, such as skatole, which exhibit a fluorescence maximum slightly shifted to either lower or higher wavelengths (Lakowicz, 2006; Ménez et al., 2018; Moradi et al., 2021). To corroborate the presence of such small organic matter in the carbonate rocks, a photobleaching test was performed by extending the acquisition time of the fluorescence spectra from 50 to 100 s (Figure 3b). This experiment resulted in a decrease in fluorescence intensity for wavelengths below 375 nm (UV range), while the intensity remained preserved at higher wavelengths (visible range). This observation supports that the UV fluorescence originates from small aromatic molecules, which can be easily degraded into radicals under UV irradiation, while the fluorescence at 420 nm, attributed to aliphatic molecules remains unaffected.

Using the monochromatic synchrotron source, the excitation wavenumber was slightly modified to further elucidate which amino acid corresponds to the fluorophores present in the carbonate rocks (Figure 3c and Figure S5 in Supplementary Information S1). Increasing the excitation wavelength from 265 to 275 nm resulted in an increase in the intensities of the fluorescence bands at 310 nm, with only a minor increase for the band at 340 nm. This phenomenon can be explained by the differences in the absorption spectrum of tyrosine and tryptophane molecules. Increasing the excitation wavelength to 275 nm significantly enhances the absorption of the tyrosine molecules, while the increase in tryptophan absorption is negligible (Lakowicz, 2006). Consequently, these observations are consistent with the presence of fluorophores exhibiting spectral similarity with tyrosine- and tryptophan-like compounds.

2.3. Elucidating the Nature of Organic Matter of Carbonate Bioclastic Grains

To get insight into the origin of the fluorescence observed in the grain components, we focused on a specific region within the Non-reservoir rock, previously identified by cross-polarized optical microscopy (see Mat&Met and Figure S6 in Supplementary Information S1). In Figure 4a, optical images from left to right reveal various components: mollusk (M), red algae (RA), foraminifera (F), echinoderm (E), and cement (C). Figure 4b presents the RGB image obtained in the fluorescence imaging microscope from emission filters R = 420–480 nm, G = 352–388 nm, and B = 329–351 nm. Additionally, Figure 4c illustrates the spectral mapping of this area, obtained by integrating the spectra from the baseline, which closely matches the fluorescence signal acquired by

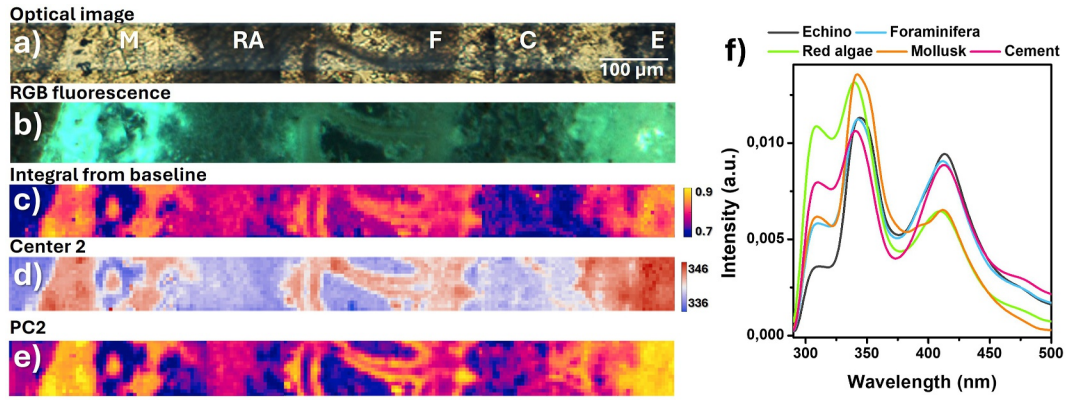

Figure 4. Fluorescence spectral mapping of various bioclastic grains of the Non-reservoir rock. (a) Optical image of the Non-rock containing the following components: mollusk (M), red algae (RA), foraminifera (F), cement (C), and echinoderm (E). Corresponding fluorescence results: (b) RGB fluorescence image (R = 420–480 nm, G = 352–388 nm, and B = 329–351 nm), (c) intensity spectral mapping, (d) center map of the peak at about 340 nm, and (e) PC2 map. (f) Representative fluorescence spectra of the different bioclastic grains of the carbonate rocks.

the filtered-emission microscope (Figure 4b). Moreover, a fitting analysis of this fluorescence mapping (Figure S7 in Supplementary Information S1) unveils that the regions with higher fluorescence intensity (mollusk, echinoderm, and foraminifera) correspond to UV emission around 340 nm (area map of Region 2 in Figure S7b in Supplementary Information S1), attributed to tryptophan-derivatives (indole moieties). UV fluorescence associated with the tyrosine compound (area map of Region 1 in Figure S7a in Supplementary Information S1) is homogeneously presented in RA and within the foraminifera cavities while heterogeneously distributed in the cement (micritic spherulites) and mollusk (bivalve). Lastly, the visible fluorescence (area map of region 3 in Figure S7c in Supplementary Information S1) is observed in the cement particles, and the echinoderm (excluding the shell).

Figure 4f shows representative spectra derived from the average of the fluorescence spectra of selected grains (N = 250–400). Fluorescence fits were conducted using six contributions: at 304 ± 2 nm, 314 ± 2 nm, 342 ± 4 nm, 382 ± 8, 412 ± 5 nm, and 440 ± 10 nm. The first four signals are assigned to UV emission peaks that are spectrally analogous to those reported for aromatic amino acids and their degradation products in reference studies, specifically to tyrosine, p-cresol (tyrosine derivative), tryptophane or indole derivative, and skatole (tryptophan derivative) (Lakowicz, 2006; Ménez et al., 2018; Moradi et al., 2021), and the two visible emissions assigned to aliphatic-rich substances (Coble, 1996; Galapate et al., 1998; Liu et al., 2020). The results indicate similar fluorescence among mollusk, foraminifera, and echinoderm skeleton remains with tryptophan residues as the main fluorophores. Interestingly, the UV fluorescence of RA exhibits more similarities to that of the cement with the predominance of tyrosine. The fitting analysis reflects the significantly higher tyrosine-to-tryptophan ratio in the RA (0.82) and the cement (0.8) compared to foraminifera (0.52), mollusk (0.45), and echinoderms (0.32). Figure S8 in Supplementary Information S1 illustrates the histograms of the peak centers resulting from the fit analysis and evidence of the differences in the emission centers between the rock components. The shifts observed between RA and cement and the other bioclastic grains are especially relevant in UV fluorescence. Among all fitting parameters, the center of the peak approximately 338–346 nm (Figure 4d) proves particularly useful in distinguishing between rock components. This shift is associated with the contribution of different molecules to this emission band (intact amino acids mixed with their derivatives). The fluorescence signal at lower wavelength corresponds to indole molecules, the degradation product of tryptophan amino acid. Thus, this fluorescence parameter provides information about organic matter preservation during rock formation and maturation.

Additionally, PCA was employed to determine which variables are more significant for explaining the fluorescence of the carbonate rocks. The Non-reservoir fluorescence maps can be explained using two components with a 95% significance. The spectra of each component and the corresponding maps for each component are presented in Figure S9 in Supplementary Information S1. The first contribution (PC1), covering 70% of the weight, indicates that the fluorescence intensity in the visible range is inversely proportional to that in the UV range. The

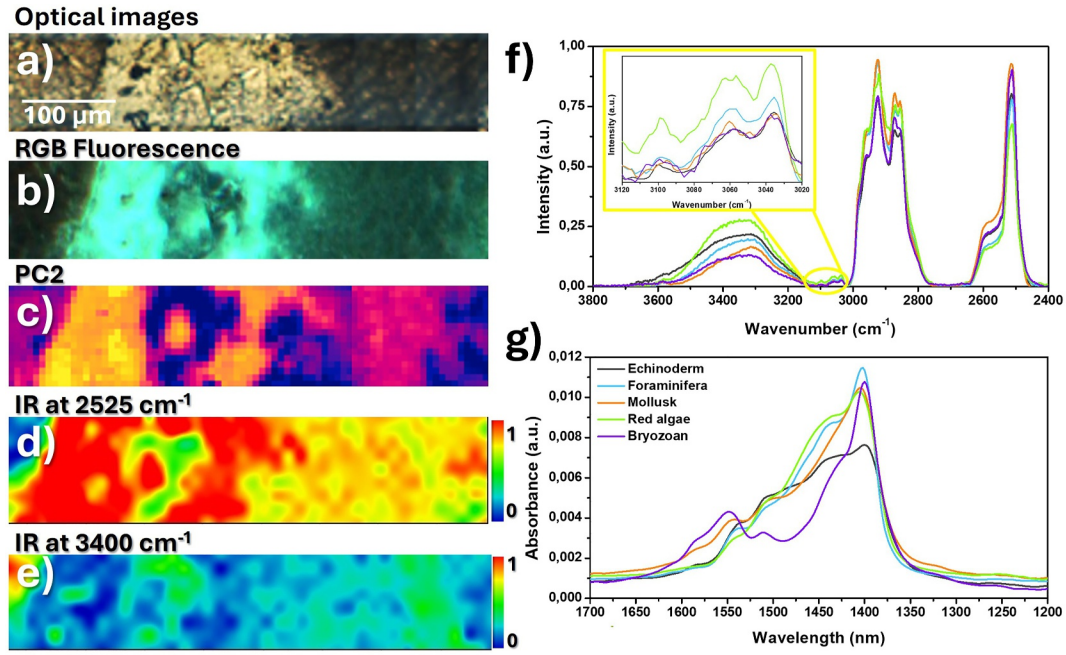

Figure 5. Fourier transform infrared (FTIR) spectral mapping of the bioclastic grains in Non-reservoir rock. (a) Optical images of the Non-reservoir rock containing a mollusk and red algae component. Corresponding fluorescence results from (b) RGB fluorescence image and (c) PC2 map and FTIR center maps at (d) 2,525 and (e) 3,400 cm^{-1}, and IR spectra of different rock components in the ranges of (f) 3,800–2,400 cm^{-1} and (g) 1,700–1,200 cm^{-1}, respectively.

second contribution (PC2), covering 25% of the component weight, contains information on the transition range of the PC1, from 350 to 400 nm. This map (Figure 4e) aligns with the fluorescence intensity maps and the area and center maps of the peak around 340 nm, indicating that this peak represents the most prominent fluorescence feature of the carbonate rock components and is ascribed to tryptophan residues.

To explore the distinct organic compositions of representative bioclastic grains, such as RA and mollusks (Figure 5a), specific regions were also subjected to analysis by FTIR microspectroscopy using synchrotron radiation. IR spectra measurements were collected in transmission mode within the range of 3,800–2,400 cm^{-1} to avoid the signal corresponding to the glass substrate vibrations. These FTIR measurements, with high spectral resolution and wide spectral domain, facilitated the analysis of overtones of carbonate vibrations, and vibrations of organic functional groups. For efficient comparison of the IR results with the fluorescence results, RGB fluorescence image and PCA map of component 2 from Figures 4b and 4e are included in Figures 5b and 5c. In addition, Figures 5d and 5e present the FTIR intensity mapping for the center at 2,525 and 3,400 cm^{-1}, respectively. The former signal corresponds to the calcite overtone vibration (a combination of the Ca-O and carbonate stretchings at 875 and 1,410 cm^{-1} bands) while the latter signal at 3,100–3,650 cm^{-1} is attributed to OH and NH stretching vibrations (Ben et al., 2011). The lower calcite signal in RA than that in mollusks may be attributed to lower calcite crystal sizes, which exhibits a higher degree of micritization leading to crystal sizes smaller than 1 µm. Interestingly, the IR signal at 3,400 cm^{-1} presents the same spatial distribution as the fluorescence signal around 290–325 nm.

Representative FTIR spectra of different bioclastic grains measured in the Non-reservoir rock are presented in Figure 5f, revealing four IR absorption bands. The first band at 2,600–2,400 cm^{-1} corresponds to the combination of calcite vibrations (875 and 1,500–1,400 cm^{-1} bands) and is remarkably similar among all the grains. The band at 3,000–2,800 cm^{-1} corresponds to the overlapping of aliphatic CH stretching signals (symmetric and asymmetric CH_2 and CH_3 stretching) and the harmonic vibrations of the 1,500–1,400 cm^{-1} band of the calcite (Loron et al., 2022). Although the former band is characteristic of organic matter, the measurements obtained in transmission mode include IR features of the glue used to mount the limestone on the glass substrate. The spectrum of the glue was measured separately (Figure S10 in Supplementary Information S1), revealing the presence of CH_2 and CH_3 signals, albeit in different proportions compared to those observed in the carbonate rock.

To estimate the relative CH_2/CH_3 concentration, a fit analysis of the IR spectra in the CH aliphatic region was conducted to calculate the differences between the glue and the carbonate bioclastic grains. The spectra were deconvoluted into 7 peaks (Figure S11 in Supplementary Information S1) with maxima at 2,825 cm^{-1} (calcite harmonic), 2,850 cm^{-1} (symmetric CH_2 stretching), 2,870 cm^{-1} (calcite harmonic), 2,895 cm^{-1} (symmetric CH_3 stretching), 2,925 cm^{-1} (asymmetric CH_2 stretching), 2,964 cm^{-1} (asymmetric CH_3 stretching) and 2,985 cm^{-1} (calcite harmonic) (Coates, 2006; Loron et al., 2022). The latter peak appears exclusively in the bioclastic grains (not in the glue spectra). Furthermore, by using the ratio between the integrated area for the band at 2,925 and 2,964 cm^{-1} (from CH_2 and CH_3, respectively), a higher methylene CH_2 signal is found in the carbonate rock than in the glue material. Interestingly, three small IR absorption peaks at 3,035, 3,058, and 3,098 cm^{-1} (inset of Figure 5f) exclusively appear in the bioclastic grains of the carbonate rock. These signals are ascribed to aromatic CH stretching vibrations but may also represent NH stretching vibrations of amino acid residues (Loron et al., 2022).

Finally, Figure 5g presents the Optical-PhotoThermal Infrared microspectroscopy analysis of bioclastic grains measured at lower wavenumbers by using reflection mode (see Mat&Met). All samples exhibit a broad IR band between 1,350 and 1,600 cm^{-1}, with notable differences in the intensity signals contributing to these bands. Fit analysis of the IR spectra was conducted using 6–7 bands (Figure S12 in Supplementary Information S1 and the assignment described in Table S3 in Supplementary Information S1). The results reveal a main band at 1,350–1,500 cm^{-1} attributed to calcite. Signals above this range are attributed to organic features, and their relative contribution differs between rock components. For example, the signal at 1,465 cm^{-1} corresponding to asymmetric CH bending in aliphatic, is absent in bryozoans. Aromatic C=C and C=N signals, appearing at 1,545 and 1,585 cm^{-1}, are significant in bioclastic grains, especially in bryozoans and mollusks. These results are in concordance with the presence of small aromatic and *N*-rich amino acid residues.

3. Discussion

This study presents a detailed spectral characterization of carbonate rock focusing on exploring the spatial distribution and spectral characteristics of organic matter in both bioclastic and non-bioclastic components. Fluorescence analysis, combining filtered emission fluorescence images and spectral fluorescence mapping, revealed distinct patterns between the Non-reservoir and Reservoir rocks. In the Non-reservoir rock, fluorescence intensity is predominantly localized within bioclastic grains, suggesting a preferential preservation of organic matter within biomineral fragments. Conversely, the Reservoir rock exhibits a more widespread fluorescence across both bioclastic and non-bioclastic grains, with enhanced signals still localized in the bioclastic grains. These spatial differences underscore the heterogeneous distribution of organic compounds in carbonate rocks, reflecting variations in their depositional and diagenetic processes.

The spectral origin of fluorescence further elucidates the nature of preserved organic molecules. UV fluorescence (300–350 nm) in carbonate rocks, primarily localized in bioclastic grains, displays spectral features comparable to those reported for small aromatic fluorophores commonly linked to biologically derived organic matter, including tyrosine- and tryptophan-like compounds and their degradation products. In contrast, visible fluorescence (420–480 nm), more prominent in the Reservoir rock, exhibits broader emission features consistent with larger aliphatic-rich compounds. These molecules not only exhibit fluorescence but are also known to enhance oil adsorption capacity. While these spectral similarities do not provide direct molecular identification, they suggest the coexistence of multiple organic phases with distinct spectral behaviors. Together, these observations reveal a complex organic matter composition of the carbonate rocks and emphasize the importance of accounting for both biotic and abiotic factors in the rock fluorescence characterization.

Infrared microspectroscopy provided complementary insights into the functional group composition of the organic matter and supports the fluorescence findings. The presence of NH and OH stretching vibrations at ~3,400 cm^{-1} and the absence of the amide I band at ~1,650 cm^{-1} support that intact proteins are unlikely to be a major component of the preserved organic matter. Instead, the IR signatures are consistent with nitrogen-bearing and aromatic functional groups present in altered or degraded organic material. Importantly, the spatial distribution of these IR features closely mirrors the UV fluorescence maps, reinforcing the interpretation that the observed spectroscopic signals reflect genuine heterogeneity in organic matter distribution rather than analytical artifacts. Notably, variations in spectral features among bioclastic components, such as higher relative

contribution of tyrosine-like emission in RA compared to foraminifera, mollusk, and echinoderm, further illustrate the influence of biomineral type and texture on organic matter preservation.

The selective photobleaching behavior observed during prolonged low-power UV irradiation provides additional constraints on the nature of the fluorophores contributing to the UV emission. The progressive decrease in UV fluorescence intensity, in contrast to the relative stability of the visible emission, is consistent with the presence of small aromatic fluorophores that are known to undergo photochemical degradation. Highly condensed or polymerized organic matter, as well as inorganic luminescence centers intrinsic to calcite, are generally more photostable under comparable conditions. Although this behavior does not exclude contributions from inorganic luminescence or high–molecular-weight organic phases, it suggests that small aromatic moieties play a significant role in the UV fluorescence observed in these samples.

These molecular signatures directly correlate with previously observed nanoscale wettability patterns in these rocks. Hydrophobic domains—primarily in bioclastic grains—are associated with enhanced UV fluorescence within bioclastic grains, supporting the hypothesis that residual organic matter influences rock-fluid interfacial behavior. Thus, the spectroscopic results not only shed light on organic matter composition, distribution and preservation, but also offer an explanation for wettability variations that critically affect fluid flow in carbonate reservoirs.

In conclusion, this integrated spectroscopic analysis provides critical insights into the nature of organic matter in carbonate rocks. The results highlight variations in the distribution and preservation of organic matter in both Reservoir and Non-reservoir carbonate rocks, influenced by bioclastic composition. The distinct UV fluorescence patterns enable differentiation among bioclastic grains, with UV emission serving as a distinguishing feature for certain types of bioclastic grains. These insights highlight the interplay between the carbonate composition and its surface chemistry, fundamental for understanding physical and chemical processes taking place at the mineral-water interface. These insights improve our understanding of carbonate diagenesis, organic matter preservation, and paleoenvironmental reconstructions, opening avenues for geological and environmental applications. Future studies integrating direct molecular analyses, such as extractable organic matter or amino acid measurements, will be essential to validate, interpret and represent an important next step beyond the scope of the present study proposed here.

Conflict of Interest

The authors declare no conflicts of interest relevant to this study.

Data Availability Statement

Data from the DISCO and SMIS beamlines of the SOLEIL synchrotron were used in this study. The dataset includes optical micrographs and raw synchrotron data (fluorescence and infrared) from the Non-reservoir and Reservoir carbonate rocks. These data are available at the Zenodo repository via https://doi.org/10.5281/zenodo.15618906, under a Creative Commons Attribution 4.0 International license. Fitting and PCA of the fluorescence hypermapping spectra associated with this manuscript were performed using Quasar software (Toplak et al., 2021). The codes used for fluorescence analysis of the Non-reservoir versus Reservoir carbonate rock, as well as of the bioclasts in Non-reservoir rocks, are available under the MIT License and openly published on Github https://github.com/moyaac/Bioclast-synchrotron-analysis (Moya, 2025).

Acknowledgments
We thank the Synchrotron SOLEIL (Saint-Aubin, France) for beamtime on the DISCO and SMIS beamlines (project #20220467). We also thank to Nicolas Agenet from Total Energies for initiating the work providing the samples and enabling this study as well as for the fruitful discussions.

References

Ben, T., Ren, H., Ma, S., Cao, D., Lan, J., Jing, X., et al. (2011). Calcite formation in soft coral sclerites is determined by a single reactive extracellular protein. *Journal of Biological Chemistry*, *286*(36), 31638–31649. https://doi.org/10.1074/jbc.M109.070185

Bisse, S. B., Ekoko, B. E., Gerber, J., Ekomane, E., & Franchi, F. (2022). Influence of biotic vs abiotic processes on the genesis of non-marine carbonates along the Cameroon Volcanic Line (Cameroon) and palaeofluid provenance. *The Depositional Record*, *8*(1), 102–126. https://doi.org/10.1002/dep2.154

Bjørlykke, K. (2014). Relationships between depositional environments, burial history and rock properties. Some principal aspects of diagenetic process in sedimentary basins. *Sedimentary Geology*, *301*, 1–14. https://doi.org/10.1016/j.sedgeo.2013.12.002

Boggs, S., Jr. (2006). *Principles of sedimentology and stratigraphy* (4th ed.). Pearson Education Inc.

Bunkin, A. F., Pershin, S. M., Artemova, D. G., Gudkov, S. V., Gomankov, A. V., Sdvizhenskii, P. A., et al. (2023). Fossil plant remains diagnostics by laser-induced fluorescence and raman spectroscopies. *Photonics*, *10*(1), 15. https://doi.org/10.3390/photonics10010015

Chiriboga, L., Xie, P., Yee, H., Vigorita, V., Zarou, D., Zakim, D., & Diem, M. (1998). Infrared spectroscopy of human tissue. I. Differentiation and maturation of epithelial cells in the human cervix. *Biospectroscopy*, *4*(1), 47–53. https://doi.org/10.1002/(SICI)1520-6343(1998)4:1<47::AID-BSPY5>3.0.CO;2-P

Coates, J. (2006). Interpretation of Infrared Spectra, A practical approach. In *Encyclopedia of analytical chemistry*. https://doi.org/10.1002/9780470027318.a5606

Coble, P. G. (1996). Characterization of marine and terrestrial DOM in seawater using excitation-emission matrix spectroscopy. *Marine Chemistry*, *51*(4), 325–346. https://doi.org/10.1016/0304-4203(95)00062-3

Galapate, R. P., Baes, A. U., Ito, K., Mukai, T., Shoto, E., & Okada, M. (1998). Detection of domestic wastes in Kurose river using synchronous fluorescence spectroscopy. *Water Research*, *32*(7), 2232–2239. https://doi.org/10.1016/S0043-1354(97)00426-0

Harms, T. K., Groffman, P. M., Aluwihare, L., Craft, C., Wieder, W. R., Hobbie, S. E., et al. (2021). Patterns and trends of organic matter processing and transport: Insights from the US long-term ecological research network. *Climate Change Ecology*, *2*, 100025. https://doi.org/10.1016/j.ecochg.2021.100025

Jin, J., & Zimmerman, A. R. (2010). Abiotic interactions of natural dissolved organic matter and carbonate aquifer rock. *Applied Geochemistry*, *25*(3), 472–484. https://doi.org/10.1016/j.apgeochem.2009.12.012

Khan, S. A., Khan, S. B., Khan, L. U., Farooq, A., Akhtar, K., & Asiri, A. M. (2018). Fourier transform infrared spectroscopy: Fundamentals and application in functional groups and nanomaterials characterization. In S. K. Sharma (Ed.), *Handbook of materials characterization* (pp. 317–344). Springer International Publishing. https://doi.org/10.1007/978-3-319-92955-2_9

Konhauser, K. O. (2009). *Introduction to geomicrobiology*. John Wiley and Sons.

Lakowicz, J. R. (Ed.) (2006)., *Principles of Fluorescence spectroscopy*. Springer. https://doi.org/10.1007/978-0-387-46312-4

Lim, M., Han, G.-C., Ahn, J.-W., & You, K.-S. (2010). Environmental remediation and conversion of carbon dioxide (CO2) into useful green products by accelerated carbonation technology. *International Journal of Environmental Research and Public Health*, *7*(1), 203–228. https://doi.org/10.3390/ijerph7010203

Liu, D., Yu, H., Yang, F., Liu, L., Gao, H., & Cui, B. (2020). Characterizing humic substances from native halophyte soils by Fluorescence spectroscopy combined with parallel factor analysis and canonical correlation analysis. *Sustainability*, *12*(23), 9787. https://doi.org/10.3390/su12239787

Loron, C. C., Sforna, M., Borondics, F., Sandt, C., & Javaux, E. J. (2022). Synchrotron FTIR investigations of kerogen from Proterozoic organic-walled eukaryotic microfossils. *Vibrational Spectroscopy*, *123*, 103476. https://doi.org/10.1016/j.vibspec.2022.103476

Ma, Y., Yi, S., & Wang, M. (2024). Biomimetic mineralization for carbon capture and sequestration. *Carbon Capture Science and Technology*, *13*, 100257. https://doi.org/10.1016/j.ccst.2024.100257

Martin, J. B. (2017). Carbonate minerals in the global carbon cycle. *Chemical Geology*, *449*, 58–72. https://doi.org/10.1016/j.chemgeo.2016.11.029

Matei, C., Berger, D., Dumbrava, A., Radu, M. D., & Gheorghe, E. (2020). Calcium carbonate as silver carrier in composite materials obtained in green seaweed extract with topical applications. *Journal of Sol-Gel Science and Technology*, *93*(2), 315–323. https://doi.org/10.1007/s10971-019-05145-6

Ménez, B., Pisapia, C., Andreani, M., Jamme, F., Vanbellingen, Q. P., Brunelle, A., et al. (2018). Abiotic synthesis of amino acids in the recesses of the oceanic lithosphere. *Nature*, *564*(7734), 59–63. https://doi.org/10.1038/s41586-018-0684-z

Meyers, P. A. (1997). Organic geochemical proxies of paleoceanographic, paleolimnologic, and paleoclimatic processes. *Organic Geochemistry*, *27*(5–6), 213–250. https://doi.org/10.1016/s0146-6380(97)00049-1

Moradi, M., Soleymani, J., Tayebi-Khosroshahi, H., Khoubnasabjafari, M., & Jouyban, A. (2021). Simple determination of p-Cresol in plasma samples using Fluorescence spectroscopy technique. *Iranian Journal of Pharmaceutical Research : IJPR*, *20*(2), e124329–e124378. https://doi.org/10.22037/ijpr.2020.114330.14799

Moya, A. (2025). Characterization of the Nature of organic matter in Carbonate Rocks implications for geological and environmental studies [Dataset]. *Zenodo*. https://doi.org/10.5281/zenodo.15618907

Moya, A., Giraud, F., Molinier, V., Perrette, Y., Charlet, L., Van Driessche, A., & Fernandez-Martinez, A. (2023). Exploring carbonate rock wettability across scales: Role of (bio)minerals. *Journal of Colloid and Interface Science*, *642*, 747–756. https://doi.org/10.1016/j.jcis.2023.03.197

Pâris, I., Petitjean, P., Rollinde, E., Aubourg, E., Busca, N., Charlassier, R., et al. (2011). A principal component analysis of quasar UV spectra at z ∼ 3⋆. *A & A*, *530*. A50. https://doi.org/10.1051/0004-6361/201016233

Pessarrodona, A., Franco-Santos, R. M., Wright, L. S., Vanderklift, M. A., Howard, J., Pidgeon, E., et al. (2023). Carbon sequestration and climate change mitigation using macroalgae: A state of knowledge review. *Biological Reviews*, *98*(6), 1945–1971. https://doi.org/10.1111/brv.12990

Pisapia, C., Jamme, F., Duponchel, L., & Ménez, B. (2018). Tracking hidden organic carbon in rocks using chemometrics and hyperspectral imaging. *Scientific Reports*, *8*(1), 2396. https://doi.org/10.1038/s41598-018-20890-4

Ridgwell, A., & Zeebe, R. E. (2005). The role of the global carbonate cycle in the regulation and evolution of the Earth system. *Earth and Planetary Science Letters*, *234*(3), 299–315. https://doi.org/10.1016/j.epsl.2005.03.006

Rodriguez-Blanco, J. D., Shaw, S., & Benning, L. G. (2011). The kinetics and mechanisms of amorphous calcium carbonate (ACC) crystallization to calcite, viavaterite. *Nanoscale*, *3*(1), 265–271. https://doi.org/10.1039/C0NR00589D

Toffolo, M. B., Ricci, G., Caneve, L., & Kaplan-Ashiri, I. (2019). Luminescence reveals variations in local structural order of calcium carbonate polymorphs formed by different mechanisms. *Scientific Reports*, *9*(1), 16170. https://doi.org/10.1038/s41598-019-52587-7

Tong, Y., Xiang, H., Jiang, J., & Chen, W. (2024). Interfacial interactions between minerals and organic matter: Mechanisms and characterizations. *Chemosphere*, *359*, 142383. https://doi.org/10.1016/j.chemosphere.2024.142383

Toplak, M., Read, S. T., Sandt, C., & Borondics, F. (2021). Quasar: Easy machine learning for biospectroscopy. *Cells*, *10*(9), 2300. https://doi.org/10.3390/cells10092300

Wada, N., Horiuchi, N., Nakamura, M., Nozaki, K., Nagai, A., & Yamashita, K. (2018). Controlled crystallization of calcium carbonate via cooperation of polyaspartic acid and polylysine under double-diffusion conditions in agar hydrogels. *ACS Omega*, *3*(12), 16681–16692. https://doi.org/10.1021/acsomega.8b02445

Xu, Z., & Tsang, D. C. W. (2024). Mineral-mediated stability of organic carbon in soil and relevant interaction mechanisms. *Eco-Environment and Health*, *3*(1), 59–76. https://doi.org/10.1016/j.eehl.2023.12.003

References From the Supporting Information

Dumas, P., Polack, F., Lagarde, B., Chubar, O., Giorgetta, J. L., & Lefrançois, S. (2006). Synchrotron infrared microscopy at the French synchrotron Facility SOLEIL. *International Workshop on Infrared Microscopy and Spectroscopy with Accelerator-Based Sources*, *49*(1), 152–160. https://doi.org/10.1016/j.infrared.2006.01.030

Giuliani, A., Jamme, F., Rouam, V., Wien, F., Giorgetta, J.-L., Lagarde, B., et al. (2009). DISCO: A low-energy multipurpose beamline at synchrotron SOLEIL. *Journal of Synchrotron Radiation*, *16*(6), 835–841. https://doi.org/10.1107/S0909049509034049

Jamme, F., Villette, S., Giuliani, A., Rouam, V., Wien, F., Lagarde, B., & Réfrégiers, M. (2010). Synchrotron UV fluorescence Microscopy Uncovers new probes in cells and tissues. *Microscopy and Microanalysis*, *16*(5), 507–514. https://doi.org/10.1017/S1431927610093852

Jamme, F., Kascakova, S., Villette, S., Allouche, F., Pallu, S., Rouam, V., & Réfrégiers, M. (2013). Deep UV autofluorescence microscopy for cell biology and tissue histology. *Biology of the Cell*, *105*(7), 277–288. https://doi.org/10.1111/boc.201200075

Marchetti, A., Beltran, V., Nuyts, G., Borondics, F., De Meyer, S., Van Bos, M., et al. (2022). Novel optical photothermal infrared (O-PTIR) spectroscopy for the noninvasive characterization of heritage glass-metal objects. *Science Advances*, *8*(9), eabl6769. https://doi.org/10.1126/sciadv.abl6769

Schindelin, J., Arganda-Carreras, I., Frise, E., Kaynig, V., Longair, M., Pietzsch, T., et al. (2012). Fiji: An open-source platform for biological-image analysis. *Nature Methods*, *9*(7), 676–682. https://doi.org/10.1038/nmeth.2019

Toplak, M., Birarda, G., Read, S., Sandt, C., Rosendahl, S. M., Vaccari, L., et al. (2017). Infrared Orange: Connecting hyperspectral data with machine learning. *Synchrotron Radiation News*, *30*(4), 40–45. https://doi.org/10.1080/08940886.2017.1338424